Ω^- Yields in pp Events at $\sqrt{s} = 13$ TeV Using the ALICE Detector

Henrik Pålsson

LUND
UNIVERSITY

Thesis for the degree of Bachelor of Science
Thesis advisor: Dr David Silvermyr

Made at the Division of Particle Physics in the autumn semester of 2020. Will be presented at the Department of Physics at Lund University on January 15, 2021.

Abstract

Ω^- is a baryon which is rarely produced in proton collisions. The theoretical models for how these Ω^- appear are yet not fully developed. Previous studies have shown that the experimental data did not agree with the models since more Ω^- particles appeared in the proton collisions than expected. In the LHC (Large Hadron Collider) outside Geneva, protons are accelerated to high energies and collided. The products from the collision are analyzed in the ALICE (A Large Ion Collider Experiment). The Ω^- yield is extracted by multiple methods, including side-band subtractions and peak fitting. When plotting the ratio of Ω^- yields divided by the reconstructed charged multiplicity, the ratio shows an increase in Ω^- yields much faster than the increase in average charged multiplicity.

Omega-partiklar i kollisioner mellan atomkärnor

Vid partikelacceleratorn LHC pågår ett flertal experiment. Ett av dem är ALICE-experimentet där atomkärnor kollideras. När atomkärnor slås sönder bildas ett plasma av kvarkar och gluoner. I detta kvark–gluonplasma skapas bland annat nya exotiska kvarkar. En av dessa mer exotiska kvarkar är särkvarken. När tre stycken särkvarkar förenas så bildar de en Omega-partikel. Omegan sönderfaller i sin tur till andra partiklar, som i slutändan övergår till vanlig materia.

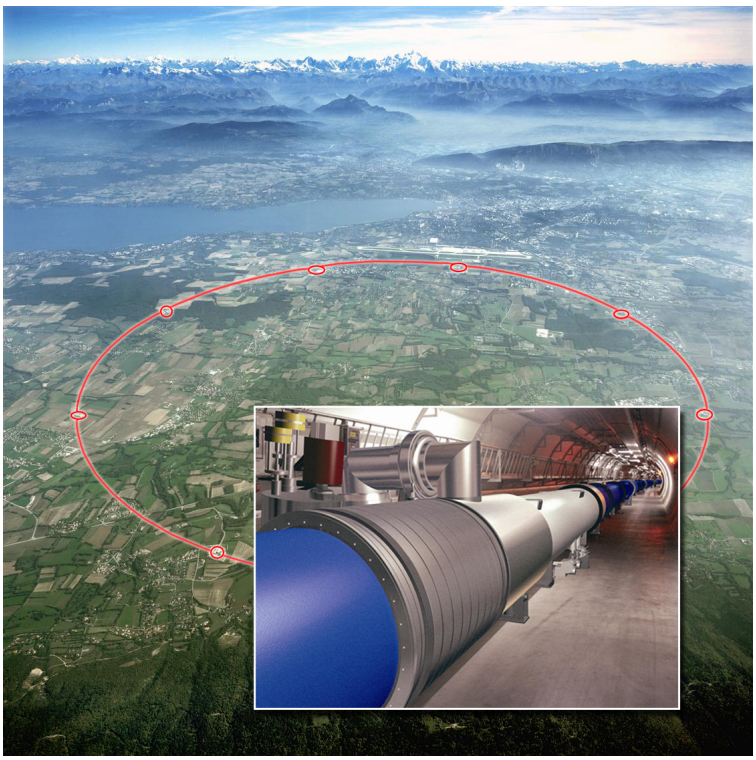

Figure 1: Partikelacceleratorn LHC ligger i tunnlar utanför Genéve [1].

Tidigare studier har visat att fler Omega bildades, än förväntat vid kollisioner mellan atomkärnor av väte. Detta arbete analyserar ny data från ALICE-experimentet tagna vid högre energinivåer än tidigare. Resultatet liknar det som observerats tidigare vid lägre energier. Förhållandet mellan Omega och laddade partiklar ökar desto mer laddade partiklar som observeras. Ökningen av Omega visar att de teoretiska modellerna behöver modifieras. Djupare analyser av kollisionerna behövs också för att förstå den bakomliggande fysiken.

Henrik Pålsson
Examensarbete 15 hp på kandidatnivå i fysik. Handledare: David Silvermyr.
Avdelningen för partikelfysik, höstterminen 2020, Lunds universitet.

Contents

1 Introduction

The Ω^- is a hadron, specifically a baryon, consisting of three strange quarks, as in Figure 2. Strange quarks do not exist in the ordinary matter on Earth, only made of up/down quarks. However, strange quarks can be produced in high energy collisions in particle accelerators. The number of strange quarks created becomes much higher when the ordinary matter undergoes a transition to a quark-gluon plasma [2]. Quark-gluon plasma is not observable directly since it exists only for a small fraction of a nanosecond. However, its decay products are possible to observe. The theoretical models for how these Ω^- appear in proton collisions are yet not fully developed. Previous studies have shown that the experimental data did not agree with the models since more Ω^- appeared in the proton collisions than expected [3, 4, 5]. In the LHC (Large Hadron Collider) outside Geneva, protons are accelerated to high energies and collided. The products from the collision are analyzed in the ALICE (A Large Ion Collider Experiment). This project will analyze reconstructed data to find a relationship between Ω^- yields and charged multiplicity.

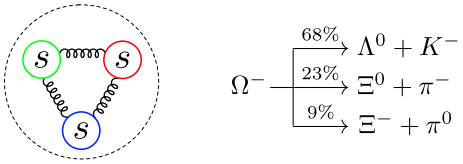

Figure 2: The Ω^- contains three strange quarks, seen to the left. Quarks are affected by the strong force mediated by gluons, here shown by the curly lines. The strong force affects several charge types, called colour charges, illustrated by red, green and blue rings around the strange quarks. To the right is the three most probable decays, with their branching ratios. Ω^- has a mean lifetime of 82 picoseconds [6], making it hard to detect directly. The decay products are traces that can be used to identify an Ω^-.

2 Background and Motivation

LHC is a particle accelerator that can recreate similar conditions as in the Big Bang [7]. Understanding the physics at those early stages of the universe might give answers about how everything might have begun, one of humanity's oldest mysteries.

2.1 The standard model

The smallest particles in the universe are the elementary particles, see Figure 3. They are not composed of other particles and have no internal structure. One can divide elementary particles into fermions and bosons; matter consists of fermions while bosons are force carriers.

Fermions consist of two subgroups: quarks and leptons. Only the quarks have colour charges that make them feel the strong force mediated by the gluon. There are six different quarks: up/down, charm/strange, top/bottom. The quarks can be combined in many ways, giving rise to a zoo of different particles. This zoo of quark combined particles is called the hadrons [9]. For example, protons and neutrons are hadrons consisting of three quarks each.

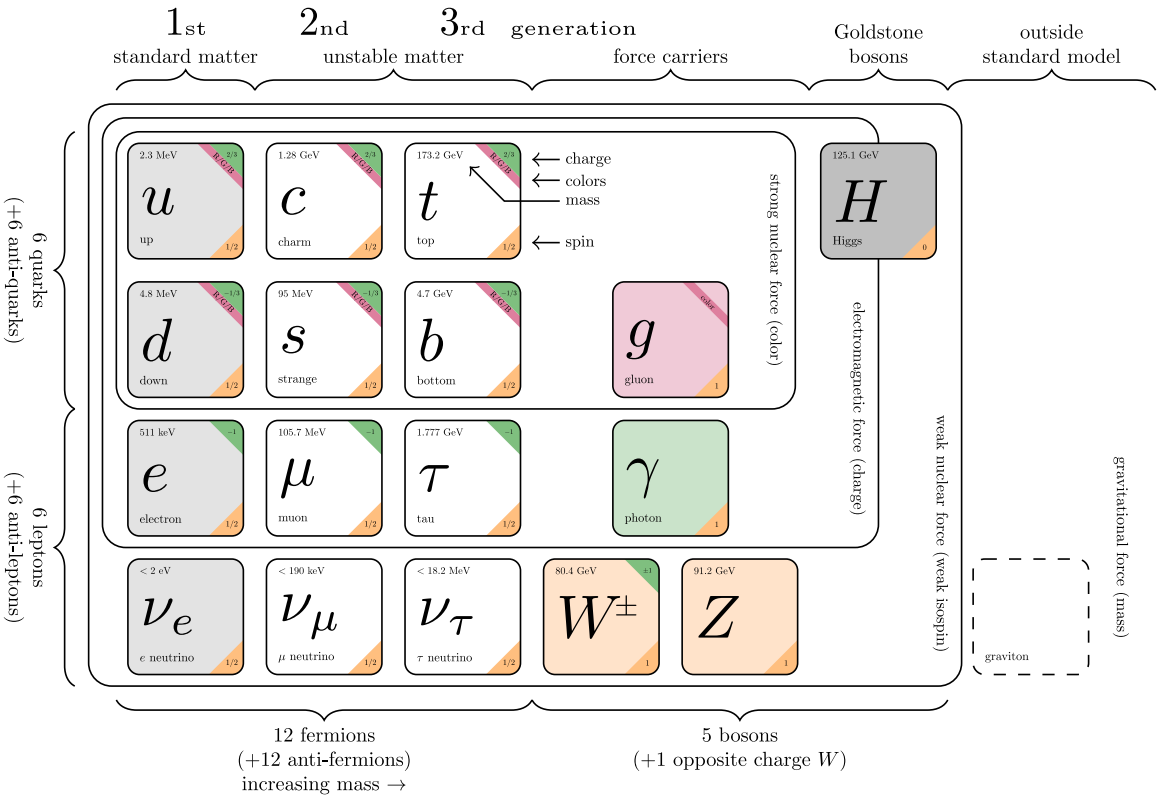

Figure 3: The standard model of elementary particles [8]. The strange quark s which builds up the Ω^-, are in generation II of the fermions.

2.2 The Ω^- baryon

Ω^- is a hadron that is very rare in proton collisions. The Ω^- was first observed in a bubble chamber at Brookhaven National Laboratory, Figure 4. The decay $\Omega^- \longrightarrow \Xi^0 + \pi^-$ was the second most probable decay, with a branching ratio of 23% [6]. The Ω^- only exist in high energy collisions on Earth created by, for example, cosmic radiation in the atmosphere or collisions created by high energy particle accelerators.

In the proton collisions, the theoretical models did not expect an enhanced production of hadrons containing strange quarks. A hint of quark-gluon plasma's formation is the enhanced production of strange quarks [11]. However, the theoretical string-like models for particle physics, e.g. Pythia predict that no quark-gluon plasma will appear in the proton collisions [12].

There is research in the ALICE group at Lund University concerning several particles that contain strangeness (i.e., strange quarks) like K mesons, Λ and Ξ baryons [13, 14, 15, 16, 17]. The Ω^- particle is fascinating because it consists of three strange-quarks. As strangeness is conserved, each collision that produces an Ω^- also has to produce three anti-strange quarks. In previous research [3] higher yield rates than predicted by string-like models was observed, making further investigation interesting.

A previous master project in Lund by Lisa Vergara [18] started in 2018 to explore Ω^- production. New, improved ALICE measurements, with more statistics, can give a more profound understanding

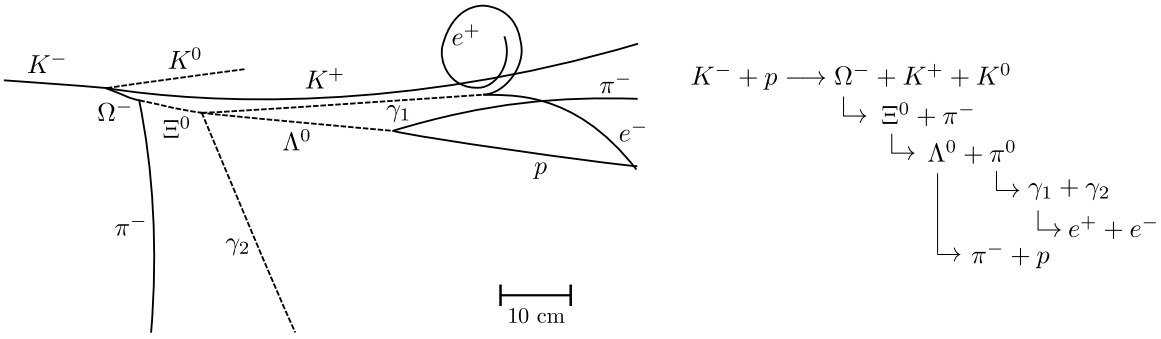

Figure 4: Bubble chamber tracks of the discovery of the Ω^- in 1964 [10]. The decay chain can be seen to the right. The tracks of neutral particles (dashed lines) are not visible in the bubble chamber. The π^0, invisible due to its short lifetime, decays into two photons (γ).

of the quark-gluon plasma. The production of strange hadrons in high-energy hadronic interactions provides a way to investigate the properties of quantum chromodynamics, i.e. the strongly interacting matter theory.

2.3 Quark-gluon plasma

Beyond two trillion degrees, the ordinary matter becomes a quark-gluon plasma like in the Big Bang. A classification based on string theory and black holes in five dimensions has made the quark-gluon plasma an archetypical strongly coupled quantum system [19]. The properties of matter in the cores of smaller neutron stars are compatible with nuclear model calculations. The interior of massive neutron stars have characteristics of the deconfined phase, which is evidence for the presence of quark-matter cores [20]. Gravitational-waves from when two neutron stars merge into a black hole also agree with the appearance of quark-matter cores [21]. Even if we can only create the Ω^- particles artificially on Earth in particle accelerators, they exist naturally in neutron stars.

2.3.1 The Big Bang

At the beginning of time, the universe was only pure energy without any particles [22]. In the first second after Big Bang, during the electroweak epoch, the strong nuclear force separated from the other forces [23]. Quark-gluon plasma and other elementary particles started to appear during this epoch [24]. At some point in this stage, an unknown mechanism called baryogenesis made an excess of matter in the order of one part in million [25]. The quark-gluon plasma epoch started when electroweak symmetry breaking made the weak and the electromagnetic force to separate [26].

3 Experiment

LHC is the largest, and most complex machine ever built and uses a network of supercomputers for collecting and processing all data from the collisions. The accelerator complex is built in tunnels about a hundred metres underground.

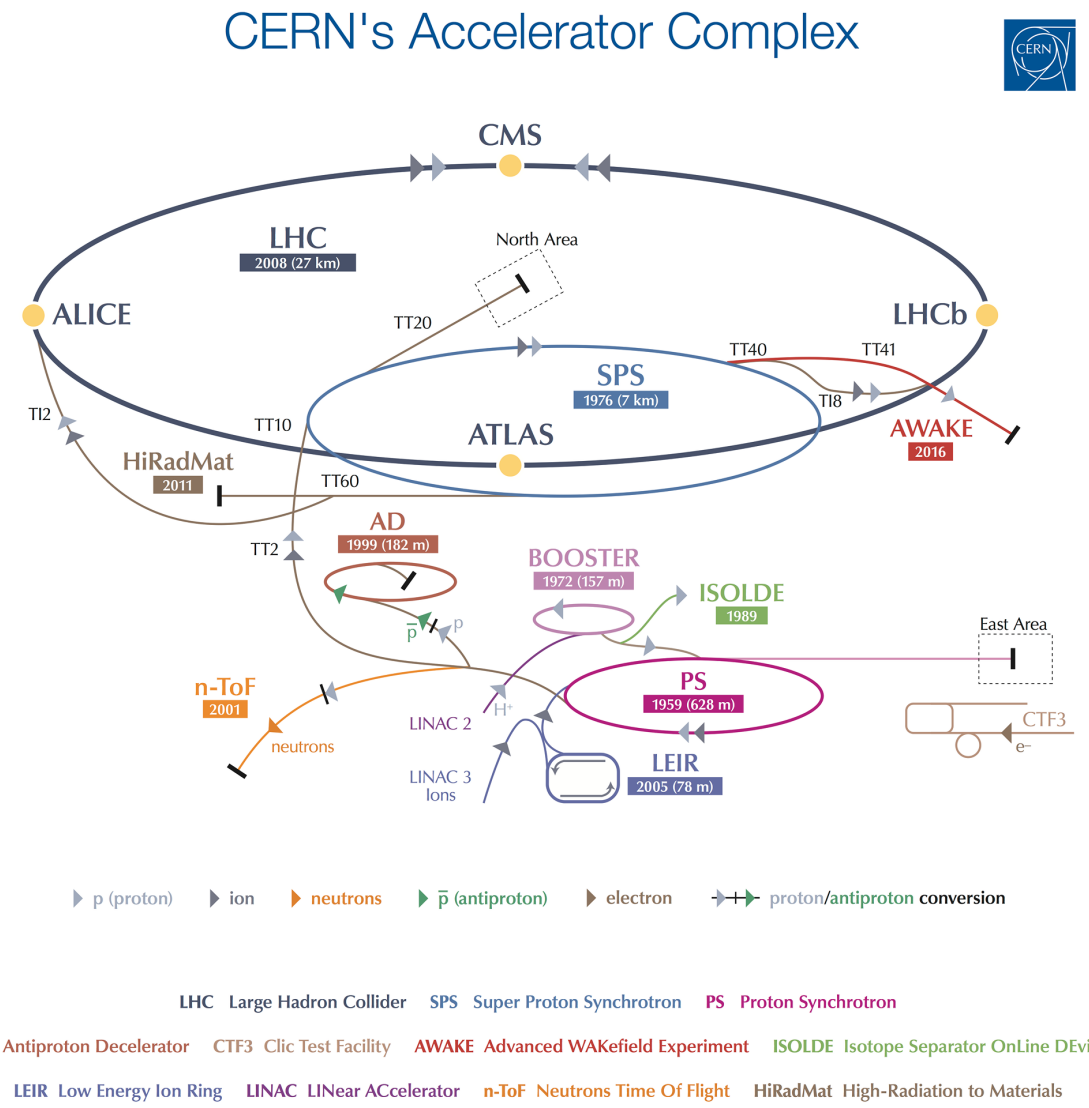

Figure 5: The CERN underground accelerator complex, located outside Geneva [1]. The LHC is the last, and largest ring (dark grey line) in a chain of particle accelerators. The smaller accelerators are used in a chain to boost the particles to their final energies and provide beams to a whole set of experiments. The ALICE detector used in this experiment is on the upper left of the LHC ring.

3.1 The Large Hadron Collider

The proton passes through several pre-accelerators, Figure 5. The collisions occur in the ALICE detector in the final accelerator ring. The source of protons is a bottle of hydrogen gas. The Linear accelerators for protons (Linac 2) use radiofrequency cavities to accelerate the protons to an energy of 50 MeV each [1].

Further, the protons enter the accelerator rings Proton Synchrotron Booster (PSB) and the Proton Synchrotron (PS). Here the protons are first accelerated to 1.4 GeV and later 25 GeV. Next, the protons enter the Super Proton Synchrotron (SPS) an accelerator ring 7 kilometres in circumference, pushing the proton beam to 450 GeV. It uses a thousand of electromagnets, including several hundred dipole magnets to bend the proton beams around the ring [1]. The proton beams leave the Proton Synchrotron at two places to get in opposite directions in the final accelerator ring.

In the final accelerator ring, LHC, the protons are accelerated to centre-of-mass energy $\sqrt{s} = 13$ TeV. The 27 kilometres long tunnel contains two parallel beam pipes in which the protons travel in opposite directions. Ten thousand superconducting magnets accelerate the proton beams. Higher multi-pole order magnets correct smaller imperfections in the field geometry [27]. Around hundred tons of superfluid helium is needed to keep the magnets, made of copper-clad niobium-titanium, near absolute zero kelvin [28].

3.2 The ALICE detector

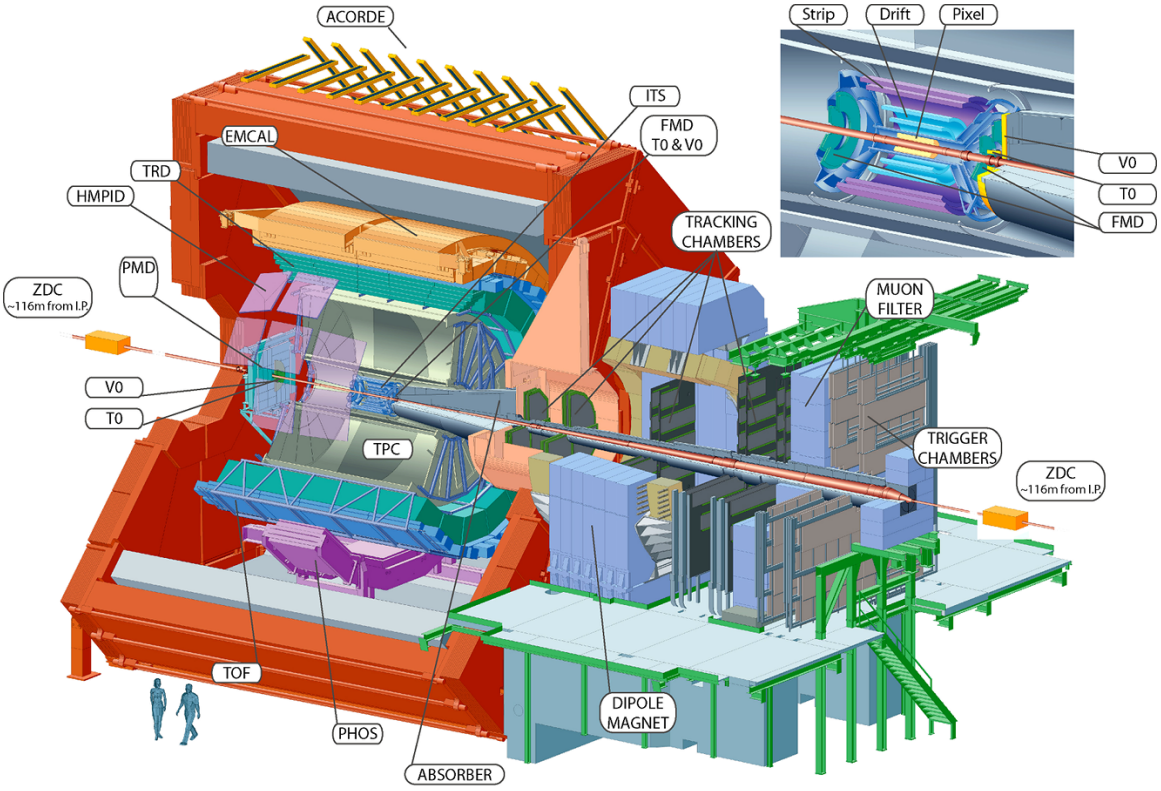

Figure 6: The ALICE detector. The Inner Tracking System (ITS), the Time Projection Chamber (TPC) and the Time Of Flight (TOF) detector are mostly used to identify the decay products $K^- + p + \pi^-$ and reconstructs their tracks from an Ω^-. The V0 detectors are used for measuring charged multiplicity N_{ch}. The coordinate system in the detector is chosen so that the beamline is along the z-axis.

In LHC the proton beams collide at four places. One is the ALICE detector, see figure 6. The other three collision places are for other experiments. The ALICE detector weighs around ten thousand tons and is in the size of a four-storey building. The analysis project is to study reconstructed cascade candidates and separate possible Ω^- signal candidates to be compared with background estimates. These Ω^- candidates are analyzed as a function of transverse momentum $p_{\mathrm{T}} = \sqrt{p_{\mathrm{x}}^2 + p_{\mathrm{y}}^2}$ and charged-particle multiplicity N_{ch} in the events. This experiment will only identifying the particles of the most common decay, seen in Figure 7. The multiplicity will be taken from the V0 detectors that use scintillators to detect charged particles from the collision.

$$
\begin{array}{l}
\Omega^- \xrightarrow{68\%} \Lambda^0 + K^- \\
\qquad\quad \Big\lfloor \xrightarrow{64\%} \mu^+ + \overline{\nu}_\mu \\
\qquad\quad \Big\lfloor \xrightarrow{64\%} p + \pi^- \Big\lfloor \xrightarrow{100\%} e^+ + \nu_e + \overline{\nu}_\mu \\
\qquad\qquad\quad \Big\lfloor \xrightarrow{99\%} \mu^+ + \overline{\nu}_\mu \\
\qquad\qquad\qquad\quad \Big\lfloor \xrightarrow{100\%} e^+ + \nu_e + \overline{\nu}_\mu
\end{array}
$$

Figure 7: The decay products to the most common Ω^- decay, with their respective branching ratios, taken from Particle Data Group [6]. The ALICE detector reconstructs tracks of protons, K^- and π^- mesons to find Ω^-.

3.2.1 The Time Projection Chamber

The time projection chamber (TPC) in ALICE gives the specific energy loss $\left\langle \frac{dE}{dx} \right\rangle$ vs. momentum for the particles from the collisions. Together with the Bethe-Bloch formula, Equation 1, the TPC can identify particles, as shown in Figure 8.

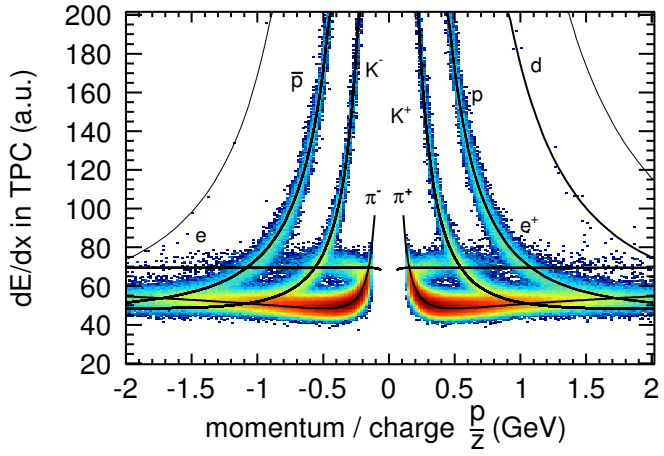

Figure 8: Specific energy loss $\left\langle \frac{dE}{dx} \right\rangle$ vs. momentum for tracks measured with the TPC in 2011 [29]. The momentum is divided by the charge of the particle, creating a negative axis for negatively charged particles.

The TPC is filled with a gas mixture of 90 % Ne and 10 % CO_2 to create avalanches from charged particles. The electrode voltage in the TPC is 100 kV and gives an electric field strength of 400 V/cm [30]. Data from the experiment has been plotted in Figure 9.

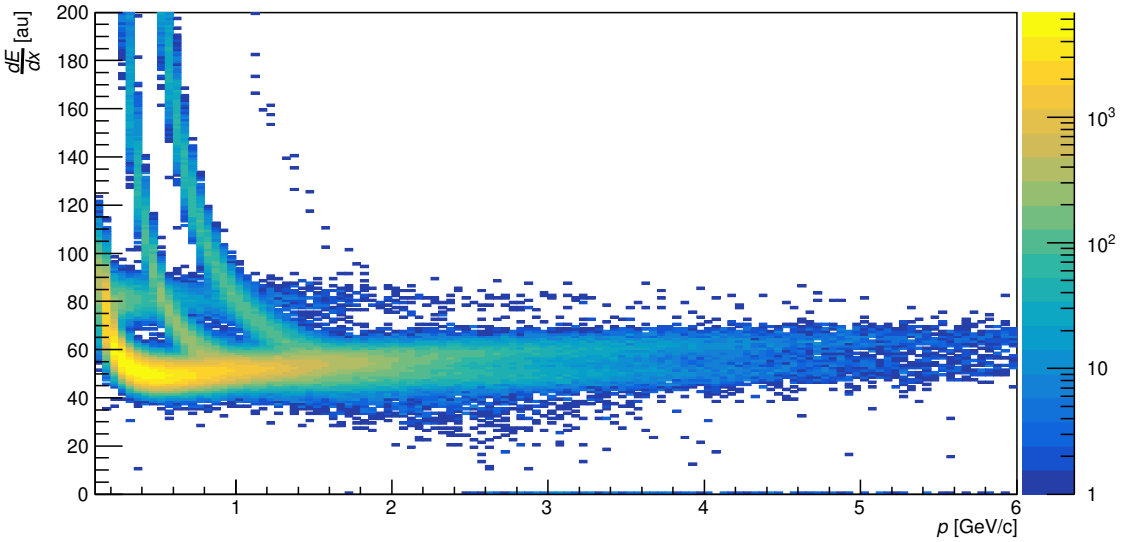

Figure 9: $\left\langle \frac{dE}{dx} \right\rangle$ in the TPC for around a hundred thousands of the events in this analysis.

The Bethe-Bloch formula [9], Equation 1, is given for a particle with energy E, travelling a distance x into the detector with the charge $\pm q$ (in units of the electron charge), speed in a fraction of the speed of light $\beta = v/c$ and the Lorentz factor $\gamma = 1/\sqrt{1-\beta^2}$.

$$\left\langle \frac{dE}{dx} \right\rangle = \frac{4\pi\alpha^2 h^2 q^2 n_e}{m_e \beta^2} \left[\ln\left(\frac{2m_e c^2 \beta^2 \gamma^2}{I} \right) - \beta^2 - \frac{\delta(\gamma)}{2} \right] \tag{1}$$

The TPC material dependent parameters are the mean excitation potential $I \approx 10Z$ eV for atomic number $Z > 20$, the dielectric screening factor $\delta(\gamma)$ and the electron density in the material n_e. Rest of the variables are constants: the speed of light c, electron rest mass m_e, the fine structure constant $\alpha \approx 1/137$ and the Planck constant h.

Instead of solving the Equation 1 analytically, the TPC uses a numerical parametrization to fit the curve $f(\beta, \gamma) \approx \left\langle \frac{dE}{dx} \right\rangle$, shown in Equation 2, in which P_i are five parameters describing $\left\langle \frac{dE}{dx} \right\rangle$ vs. momentum tracks [31], where each particle has it own set of P_i parameters.

$$f(\beta, \gamma) = \frac{P_1}{\beta^{P_4}} \left[P_2 - \beta^{P_4} - \ln\left(P_3 + \frac{1}{(\beta\gamma)^{P_5}} \right) \right] \tag{2}$$

The variables γ and β can be calculated from the momentum p and mass m of the observed particle by $\gamma = \sqrt{1 + \left(\frac{p}{mc}\right)^2}$ and $\beta = \frac{p}{\sqrt{p^2 + (mc)^2}}$ [9].

4 Results and Discussion

For a system of particles, the total invariant mass W can be calculated by $W^2c^4 = (\sum E)^2 - \|\sum \mathbf{p}c\|^2$, where E and $\mathbf{p}$ is their respectively energies and momentum [9]. The summations are over the proton+K^- + π^- reconstructed tracks to an Ω^-. The mass difference Δm_{Ω^-} is calculated by $\Delta m_{\Omega^-} = W - m_{\Omega^-}$, where $m_{\Omega^-} = 1.6725$ GeV/c^2 [6]. The yields of Ω^- from the experimental and simulated data can be seen in Figure 10 and 11.

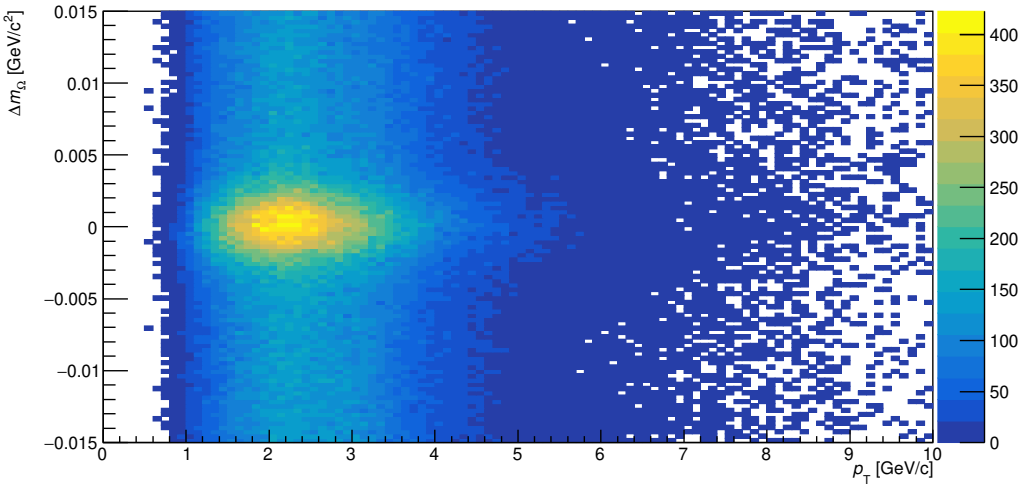

Figure 10: A half-million Ω^- candidates from 625 million events in the ALICE detector in 2018.

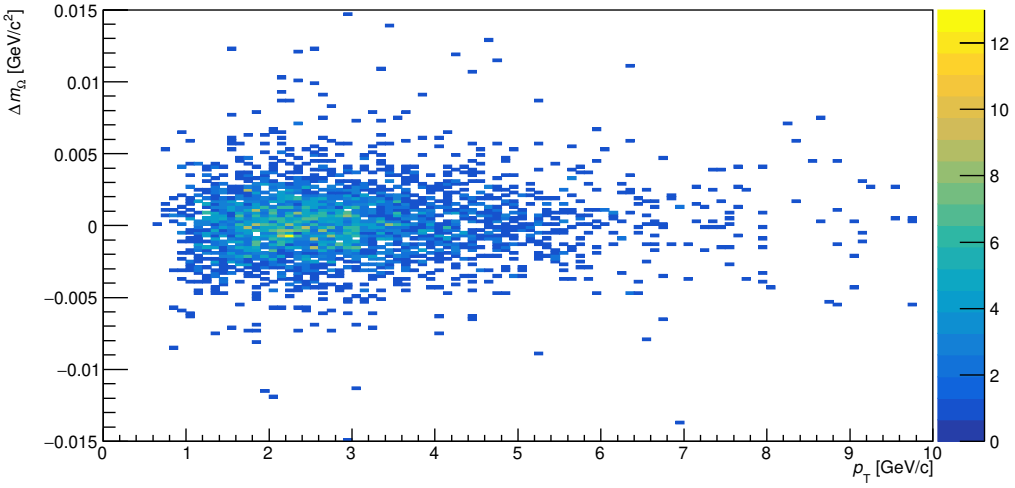

Figure 11: Three thousand Ω^- from 152 million Monte Carlo simulated events.

4.1 Analysis of events from ALICE

The ALICE data, Figure 12 and 13, shows the Ω^- divided into different bins, depending on transverse momentum p_{T} of the Ω^- candidates. We will look at the yields of Ω^- candidates divided up by event centrality in Section 4.4. The fits on the events from ALICE is calculated using the likelihood function. We have made a linear fit to the background, which comes from particles that have been wrongfully identified as the decay products of an Ω^-. The Gaussian distribution is a type of continuous probability distribution. The general form of its probability density function is given in Equation 3. The parameters μ and σ and σ^2, is the mean, standard deviation and the variance of the distribution [32].

$$f(x) = \frac{1}{\sigma\sqrt{2\pi}} \exp\left(-\frac{(x-\mu)^2}{2\sigma^2}\right) \tag{3}$$

The χ^2 statistical parameter, Equation 4, is defined as where $f(x_i)$ represents the corresponding value on the fitted curve, y_i is the experimental value, and σ_i its uncertainty [32].

$$\chi^2 = \sum_{i=1}^{k} \left(\frac{f(x_i) - y_i}{\sigma_i}\right)^2 \tag{4}$$

χ^2 divided by degrees of freedom k is a measure of how well the Gaussian fitted the data. The χ^2/k for the Gaussian fits the experimental data can be seen in Figure 14.

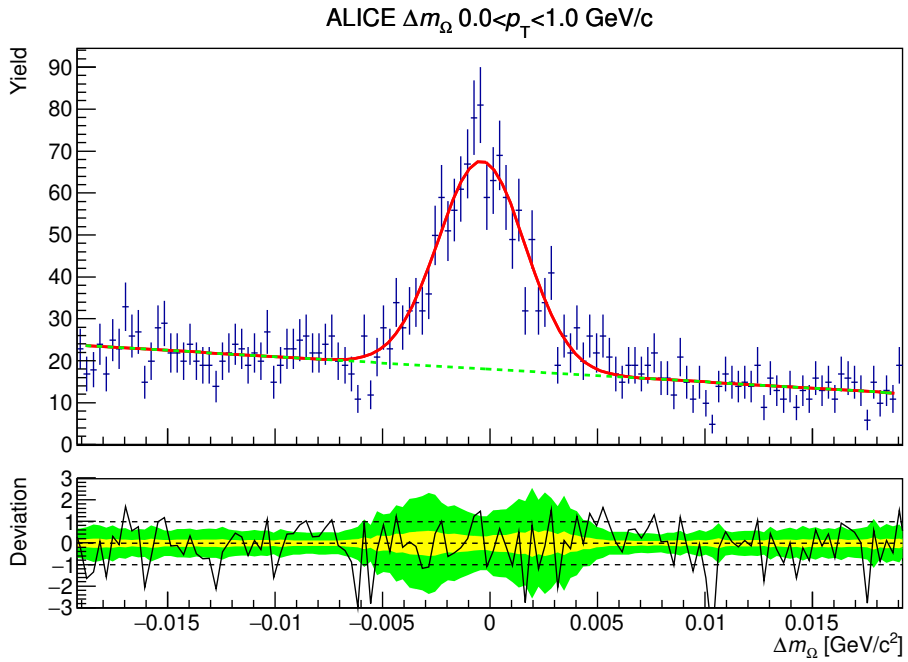

Figure 12: Gaussian fit on the experimental data from the ALICE detector. For Ω^- candidates with transverse momentum $0.0 < p_{\mathrm{T}} < 1.0$ GeV/c. The lower pad shows the residual between the fit and the data. Green colour means one sigma band and yellow means two sigma band. The solid line shows the deviation from the uncertainty of each value and the fit.

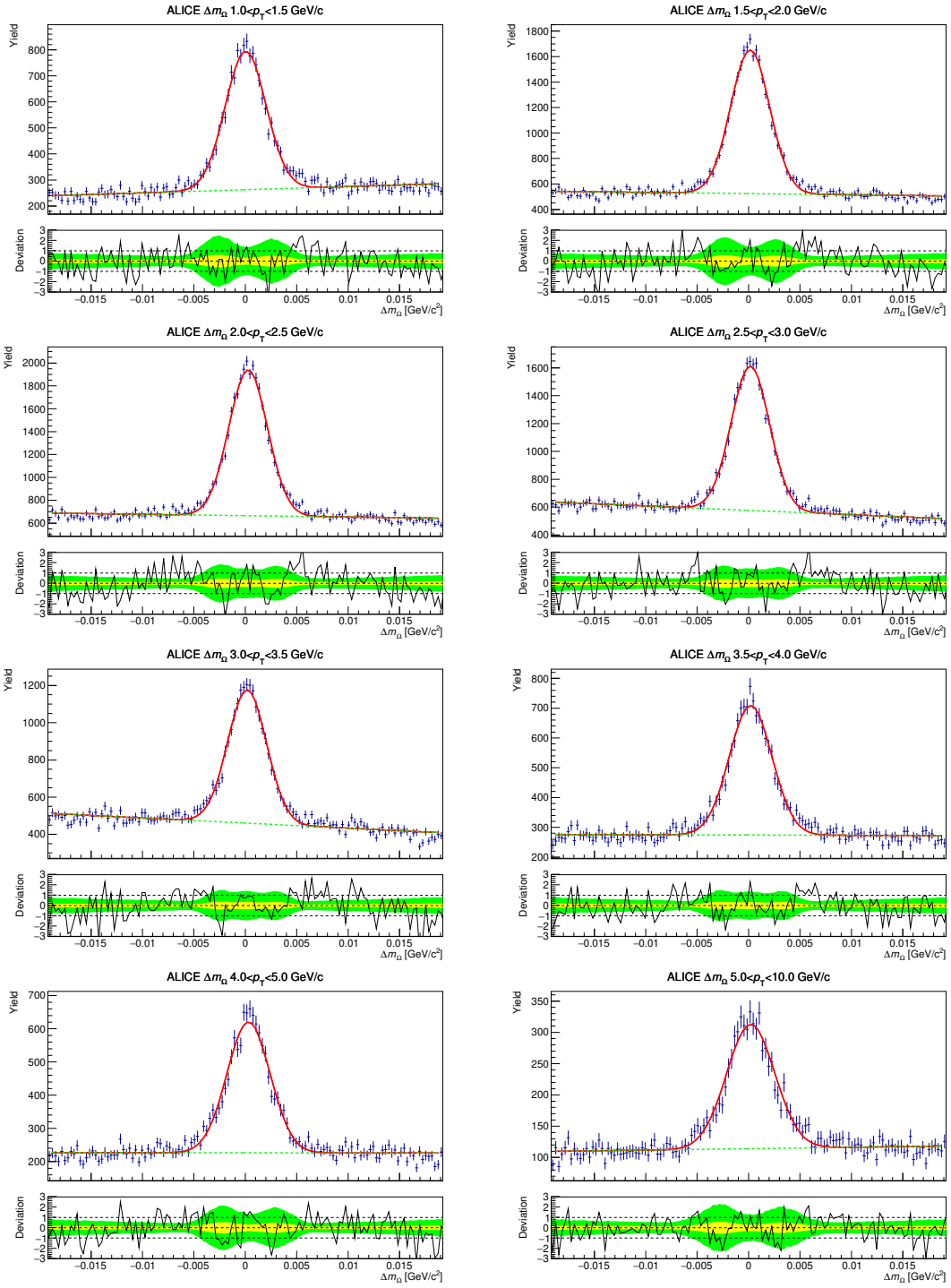

Figure 13: Gaussian (red) and linear background (green) fits on the experimental data (blue) from the ALICE detector.

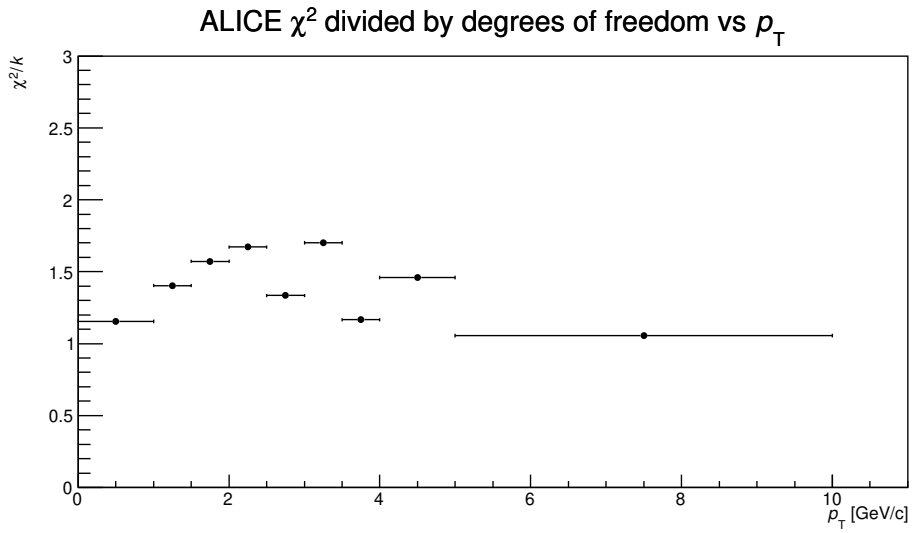

Figure 14: χ^2/k of the Gaussian fits on the experimental data.

4.2 Monte Carlo simulations

The simulations are done using Monte Carlo methods. Pythia8 is used as event generator input and GEANT-3 for full detector simulation . Pythia8 is based on the Standard Model and Lund String Model [33]. GEANT-3 simulates the passage of particles through the ALICE-detector [34]. The simulations show how collisions that produce Ω^- baryons will be observed in the ALICE detector. The simulations are divided into bins, Figure 15 and 16, depending on p_{T} of the observed Ω^-.

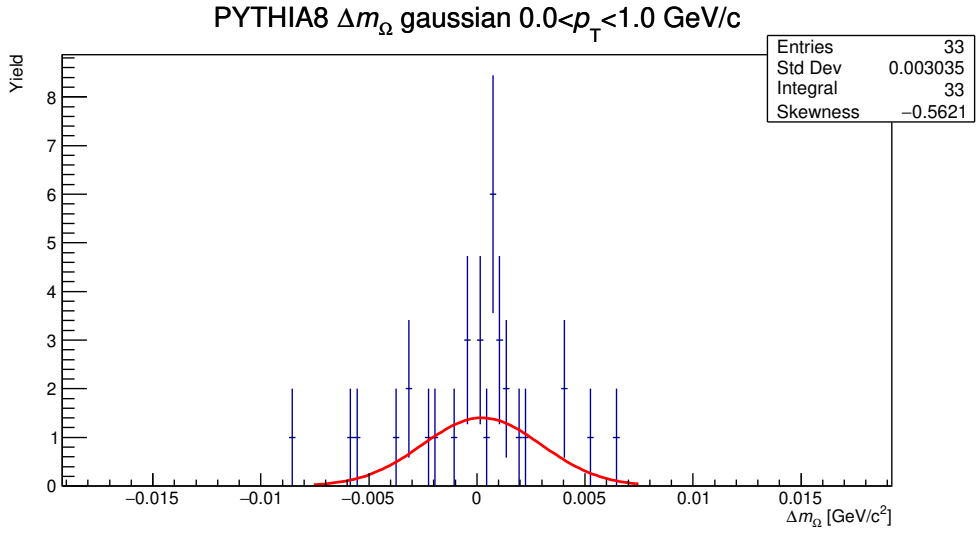

Figure 15: The blue bars are simulated Ω^- yields, and the Gaussian fit is the red curve. The statistics in the upper right corners are from the data and not the Gaussian fits.

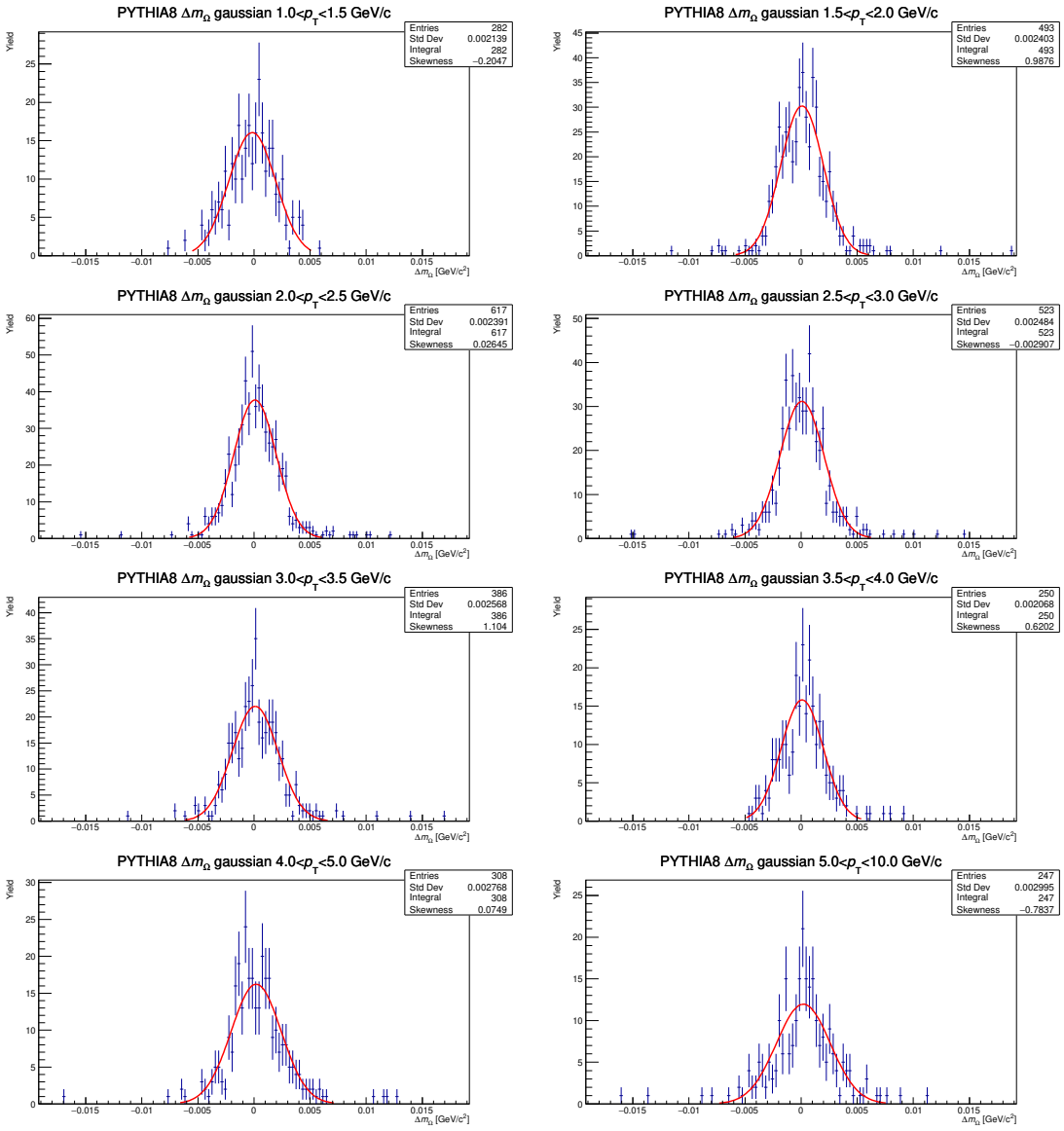

Figure 16: Yields of the simulated Ω^- in different transverse momentum p_{T}. The simulation knows if the Pythia8 event generator produces an Ω^-. Thereby, there is no background of wrongfully identified decay products.

4.3 Comparison between the Gaussian fits

The mean values μ of Δm_Ω in the Gaussian fits are in a scale of below one MeV, Figure 17. The standard deviation σ of the fits, Figure 18, show an increased standard deviation in higher transverse momentum p_{T}, both for experimental and simulated data.

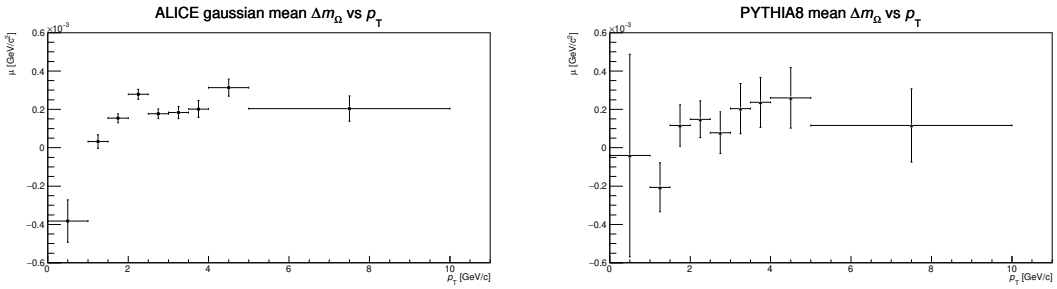

Figure 17: Comparing the mean values μ of the Gaussian fits on mass difference Δm_{Ω^-} for different p_{T}. Experimental data in the left trend and simulated data to the right.

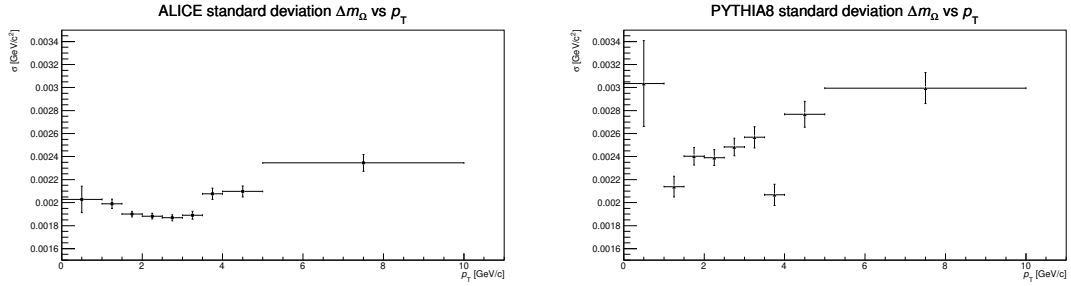

Figure 18: Comparing the standard deviations σ of the Gaussian fits on mass difference Δm_{Ω^-} for different p_{T}. Experimental data in the left trend and simulated data to the right.

4.4 Ω^- data yields as a function of centrality

For the centrality estimate, we use signals from the V0 detector, which gives a signal that is proportional to the charged-particle multiplicity. This V0 signal is normalized to a scale 0-100 called V0M. A value of 0 means that the collision was estimated to be among the most central, i.e. events with the highest observed charged-particle multiplicity. We divide up this centrality range in 5 different bins, each with 20% of the total events, as shown in Figure 19.

The rapidity y of an particle with energy E, mass m and momentum p_z along the beam line, is the hyperbolic angle $y = \tanh^{-1}(p_z/E)$. For highly relativistic particles where $p \gg m$, the rapidity y can be approximated as $y \approx -\ln\tan(\theta/2) \equiv \eta$. The approximation η is called the pseudo-rapidity and the angle θ can be obtained from the relation $\cos\theta = p_z/p$ [6]. For example, particles with trajectories $\theta = 0°$, that are parallel to the beam line has $\eta = \infty$, trajectories with $\theta = 45°$ has $\eta = 0.88$ and $\theta = 90°$ gives $\eta = 0$ [35].

Sideband subtraction method is a way to calculate yields of Ω^- if assuming that the background is linear. The signal region needs to be identified and then the regions to the left and right are then called sidebands. The signal region is contained within $|\Delta m_{\Omega^-}| \leq 6$ MeV/c^2, and the two sidebands then become 6 MeV/c^2 $< |\Delta m_{\Omega^-}| \leq 12$ MeV/c^2. By removing the yields from the sidebands in the signal region, we get an estimate of the Ω^- signal.

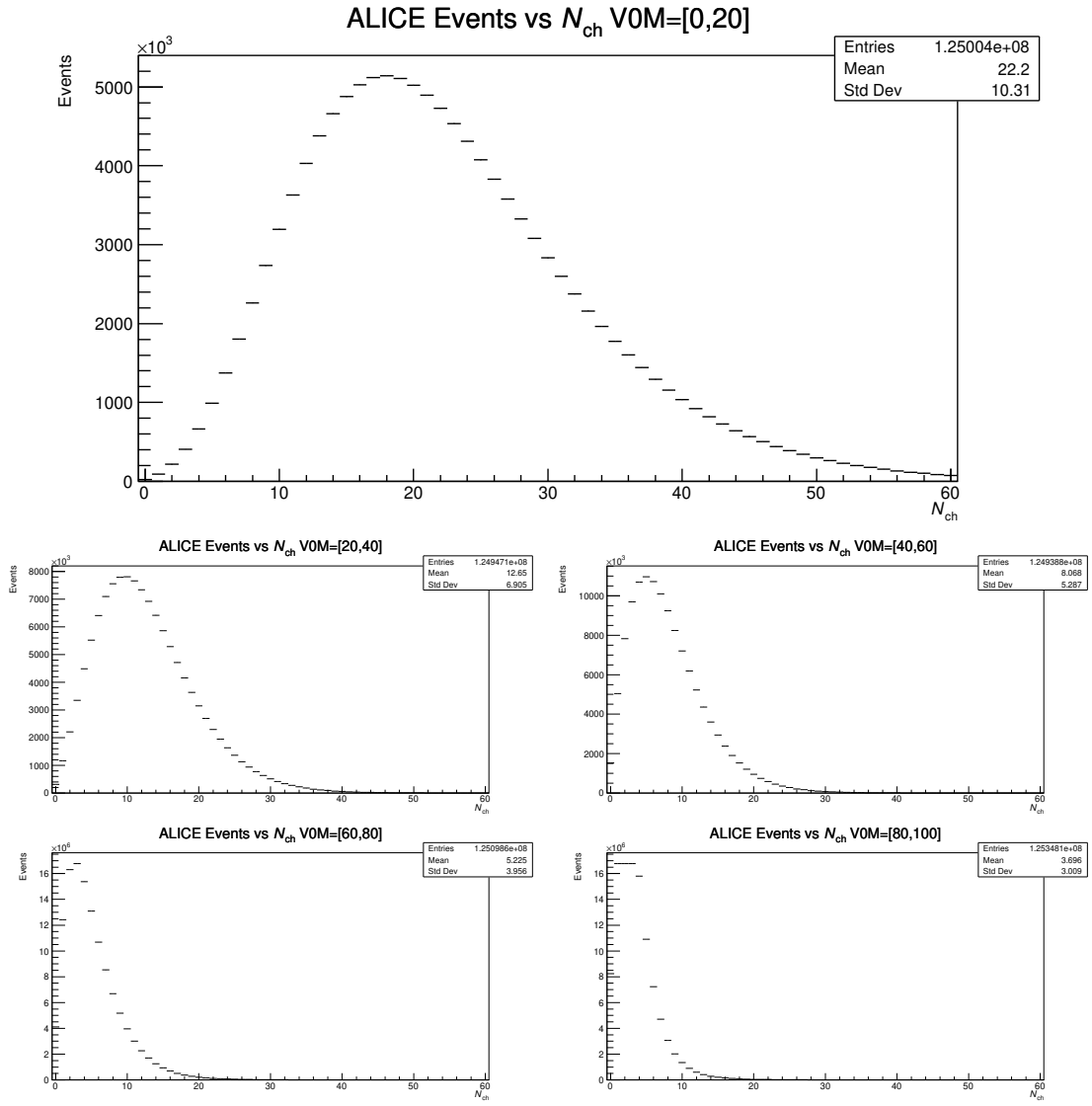

Figure 19: The distributions of events charged tracks in the ALICE detector mid-rapidity region $|\eta| < 0.8$, which is the angle covered by the TPC, compared to N_{ch} signals from the V0 detector in different 20% bins.

As seen from Figure 20, the yield of Ω^- is smaller for the most peripheral bin (80-100), and this, in particular, for the lowest and highest p_{T} bins. Therefore to compare the total yields fairly versus centrality, we only add up the yields from a limited range in $1.5 < p_{\mathrm{T}} < 4.0$. A comparison of these sums normalized by the average $\langle N_{ch} \rangle$ per centrality bin is shown in Figure 21.

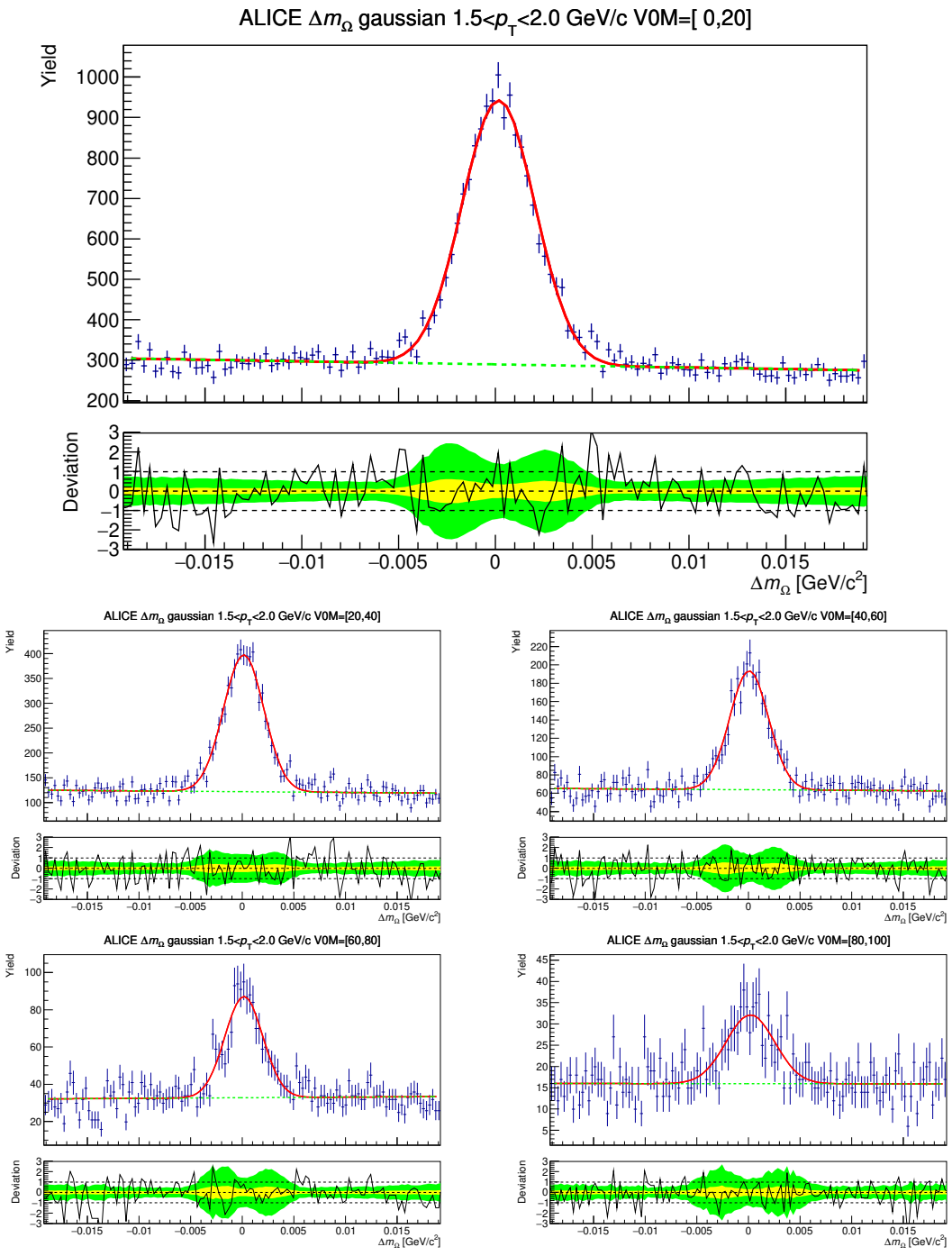

Figure 20: Example fits for invariant mass Δm_Ω for the five V0M bins. Shown for a particular bin in transverse momentum $1.5 < p_\mathrm{T} < 2.0$. The lower pad shows the residual between the fit and the histogram.

Since we do not have an absolute normalization, including acceptance and efficiency, but still want to have an idea of the centrality dependence of Ω^- production, we scaled the ratio $\frac{\Omega_{CP}}{\langle N_{ch}\rangle}$ to be 1 for the most peripheral bin $80 < V0M < 100$, indicated by the subscript CP. Figure 21 shows that the increase in Ω^- yields is much faster than the increase in average charged multiplicity $\langle N_{ch}\rangle$. The statistical errors are quite small but note that no systematic errors are included here.

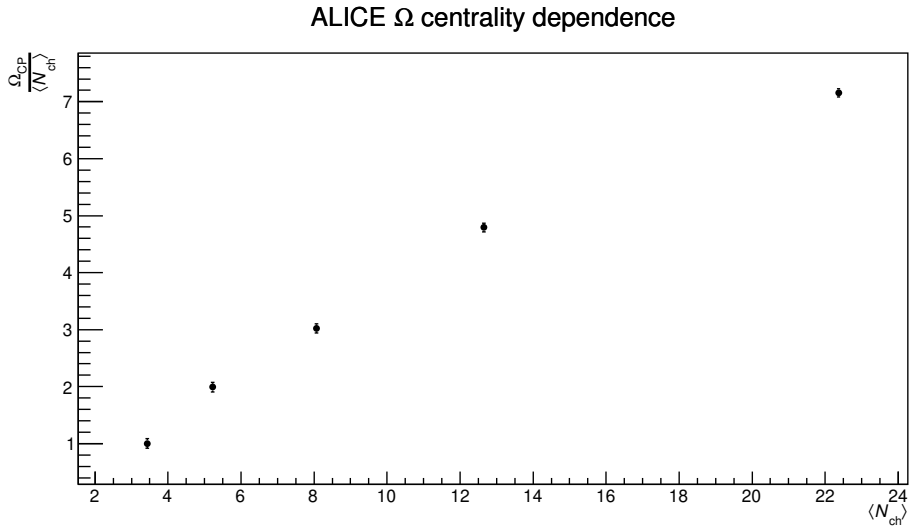

Figure 21: Increase in Ω^- yields compared to the increase in average charged multiplicity $\langle N_{ch}\rangle$.

5 Conclusion and Outlook

The ratio $\frac{\Omega_{CP}}{\langle N_{ch}\rangle}$ compared to charged multiplicity $\langle N_{ch}\rangle$ shows that the increase in Ω^- yields is much faster than the increase in average charged multiplicity $\langle N_{ch}\rangle$. The statistical errors are quite small, but no systematic errors are included here, which probably are bigger.

Due to time constraints, there are several avenues that I did not have time to pursue. A first thing to check further would be the agreement or disagreement between the Gaussian fit results and the sideband subtraction methods. Next would be to look into the overall normalization of the data results and estimate the acceptance and efficiency factors (very different for Ω^- and $N_{\rm ch}$) needed for this, in Monte Carlo simulations. If we wanted to compare with earlier published results at lower energies, we would also normalize our $N_{\rm ch}$ to be within the central unit of rapidity $|\eta| < 0.5$ only.With this, a study of different $p_{\rm T}$ cuts, to optimize signal vs background in Monte-Carlo, could be done, as well as estimation of systematic errors from the methods associated with the cuts.

Finally, I compared Ω^- with $\langle N_{ch}\rangle$. It would be interesting to compare the Ω^- yields with more specific ratios to other particles, such as $\pi^+ + \pi^-$, K, or Λ. Nevertheless, this would be more like a topic for a PhD thesis. There is thus much more work left to do before a publication of the results. However, this study shows that there is significant statistics available for an interesting measurement.

6 Acknowledgements

I want to thank my supervisor David Silvermyr for all the support, help and feedback during the whole project, and Peter Christiansen, for the ROOT scripts and the reduced trees used in my analysis. I am also extremely grateful to Omar Vazquez Rueda at the ALICE group for invaluable advice and continuous support while learning C++ and the ROOT framework. I would also like to thank Sumit Basu, Jonatan Adolfsson, Adrian Nassirpour and Oliver Matonoha at the ALICE group at Lund University for all support.

References

[1] Conseil Européen pour la Recherche Nucléaire (CERN). *The Large Hadron Collider*. Geneva, Switzerland. URL: `info.cern.ch/`.

[2] E.V. Shuryak. "Quantum chromodynamics and the theory of superdense matter". In: *Phys. Rep.* 61.71–158 (1980).

[3] J. Adam *et al.* (ALICE Collaboration). "Enhanced production of multi-strange hadrons in high-multiplicity proton–proton collisions". In: *Nature Physics* 13.535–539 (2017).

[4] S. Acharya *et al.* (ALICE Collaboration). "Multiplicity dependence of (multi-)strange hadron production in proton-proton collisions at $\sqrt{s} = 13$ TeV". In: *Eur. Phys. J. C* 80 (2020), p. 167.

[5] S. Acharya *et al.* (ALICE Collaboration). "Multiplicity dependence of $K^*(892)^0$ and $\phi(1020)$ production in pp collisions at $\sqrt{s} = 13$ TeV". In: Phys. Lett. B 807 (2020). ISSN: 0370-2693.

[6] P.A. Zyla *et al.* (Particle Data Group). "Review of Particle Physics". In: *PTEP* 2020.8 (2020), p. 083C01. DOI: `10.1093/ptep/ptaa104`.

[7] Planck Collaboration. "Planck 2015 results. XIII. Cosmological parameters". In: (2016).

[8] Carsten Burgard. *A standard diagram of the current standard model of physics*. 2016.

[9] Brian R. Martin and Graham Shaw. *Particle Physics*. 4th Edition. United Kingdom: John Wiley and Sons Ltd, 2017.

[10] V.E. Barnes *et al.* "Observation of a Hyperon with Strangeness Minus Three". In: *Phys. Rev. Lett.* 12.204 (1964).

[11] E. Andersen *et al.* (WA97 Collaboration). "Strangeness enhancement at mid-rapidity in Pb–Pb collisions at 158 A GeV/c". In: *Phys. Lett. B* 449.401–406 (1999).

[12] V. Khachatryan *et al.* (CMS Collaboration). "Evidence for collectivity in pp collisions at the LHC". In: *Phys. Lett. B* 765.193–220 (2017).

[13] Jonatan Adolfsson. *Study of Ξ-Hadron Correlations in pp Collisions at $\sqrt{s} = 13$ TeV Using the ALICE Detector*. Lund University, 2020.

[14] Maria Mårtenson. *Elliptic flow of π, K, p and φ in Pb-Pb collisions at the Large Hadron Collider*. Lund University, 2016.

[15] M. Petersson Sjögren. *Production of J/Ψ mesons in p–Pb collisions at the Large Hadron Collider*. Lund University, 2015.

[16] A.F. Nassirpour. *Production of φ Mesons as a Function of Multiplicity & Spherocity*. Lund University, 2017.

[17] M. Burheim. *Production of K^0_S and Λ in p-Pb Collisions at $\sqrt{s_{NN}} = 5.02$ TeV Measured with the ALICE Detector at the LHC*. Lund University, 2017.

[18] Lisa Vergara. *Omega Baryon Production as a Function of Multiplicity in Proton-Proton Collisions at $\sqrt{s}$ = 13 TeV*. Lund University, 2019.

[19] Barbara V. Jacak and Berndt Müller. "The Exploration of Hot Nuclear Matter". In: *Science* 337.6092 (2012).

[20] Eemeli Annala *et al.* "Evidence for quark-matter cores in massive neutron stars". In: *Nature Physics* 16.1745-2481 (June 2020), pp. 907–910. DOI: 10.1038/s41567-020-0914-9.

[21] Lukas R. Weih, Matthias Hanauske, and Luciano Rezzolla. "Postmerger Gravitational-Wave Signatures of Phase Transitions in Binary Mergers". In: *Phys. Rev. Lett.* 124 (Apr. 2020). DOI: 10.1103/PhysRevLett.124.171103.

[22] W.G. Unruh. *The early universe*. Reidel, 1988.

[23] Alan H. Guth. *The Inflationary Universe: Quest for a New Theory of Cosmic Origins*. London: Vintage Books, 1997.

[24] P. Schewe and B. Stein. "An Ocean of Quarks". In: *Physics News Update* 728.1 (2005).

[25] E. Kolb and M. Turner. *The Early Universe*. Redwood City, CA: Addison-Wesley, 1988.

[26] M. D'Onofrio and K. Rummukainen. "Standard model cross-over on the lattice". In: *Physical Review D.* 93.025003 (2016).

[27] Stephen Myers. "The Large Hadron Collider 2008-2013". In: *International Journal of Modern Physics A* 28.25 (2013).

[28] J.D. Adam *et al.* "Status of the LHC superconducting cable mass production". In: *Applied Superconductivity, IEEE Transactions on* 12 (Apr. 2002), pp. 1056–1062.

[29] K. Aamodt *et al.* "Production of pions, kaons and protons in pp collisions at $\sqrt{s} = 900$ GeV with ALICE at the LHC". In: *The European Physical Journal C* 71.6 (2011).

[30] ALICE collaboration. *A Large Ion Collider Experiment*. Geneva, Switzerland. URL: alice-collaboration.web.cern.ch/.

[31] J. Alme *et al.* "The ALICE TPC, a large 3-dimensional tracking device with fast readout for ultra-high multiplicity events". In: *Nuclear Instruments and Methods in Physics Research Section A: Accelerators, Spectrometers, Detectors and Associated Equipment* 622.1 (2010), pp. 316–367. ISSN: 0168-9002.

[32] Arne Frennelius. *Sannolikhetslära och statistisk inferens för tekniska utbildningar*. Västerås Statistikutbildning, 2004.

[33] Torbjörn Sjöstrand, Stephen Mrenna, and Peter Skands. "A brief introduction to PYTHIA 8.1". In: *Computer Physics Communications* 178.11 (2008), pp. 852–867. ISSN: 0010-4655.

[34] R. Brun *et al. Simulation program for particle physics experiments, GEANT: user guide and reference manual*. Geneva: CERN, 1978.

[35] V. Chiochia. *Accelerators and Particle Detectors*. University of Zürich, 2010.